Title

Catestatin selects for the colonization of antimicrobial-resistant gut bacterial communities

Authors

Pamela González-Dávila [1#], Markus Schwalbe [1#], Arpit Danewalia [2], Boushra Dalile [3], Kristin Verbeke[3], Sushil K Mahata [2,4$], Sahar El Aidy [1$]

Affiliations

[1] Host-Microbe Metabolic Interactions, Groningen Biomolecular Sciences and Biotechnology Institute (GBB), University of Groningen, Groningen, the Netherlands

[2] Department of Medicine, University of California San Diego, La Jolla, CA, USA.

[3] Translational Research in GastroIntestinal Disorders (TARGID), Department of chronic diseases and metabolism, Faculty of Medicine, KU Leuven, Leuven, Belgium

[4] VA San Diego Healthcare System, San Diego, CA, USA.

[#] Shared first author

[$] Shared correspondence: Sushil K Mahata, smahata@health.ucsd.edu

Sahar El Aidy, sahar.elaidy@rug.nl

Abstract

The gut microbiota is in continuous interaction with the innermost layer of the gut, namely the epithelium. Among the various functions of the gut epithelium, is to keep the microbes at bay to avoid overstimulation of the underlying mucosa immune cells. To do so, the gut epithelia secrete a variety of antimicrobial peptides, such as catestatin (CST). As a defense mechanism, gut microbes have evolved antimicrobial resistance mechanisms to counteract the killing effect of the secreted peptides. To this end, we treated wild-type mice and mice with a knockout in the CST coding region of the chromogranin-A gene (CST-KO) with CST for 15 consecutive days. CST treatment was associated with a shift in the diversity and composition of the microbiota in the CST-KO mice. This effect was less prominent in WT mice. Levels of the microbiota-produced short-chain fatty acids, in particular, butyrate and acetate were significantly increased in CST-treated CST-KO mice but not the WT group. Remarkably, both CST-treated CST-KO and WT mice showed a significant increase in microbiota-harboring phosphoethanolamine transferase-encoding genes, which facilitate their antimicrobial resistance. Finally, we show that CST was degraded by *Escherichia coli* via an omptin-protease and that the abundance of this gene was significantly higher in metagenomic datasets collected from patients with Crohn's disease but not with ulcerative colitis. Overall, this study illustrates how the endogenous antimicrobial peptide, CST, shapes the microbiota composition in the gut and primes further research to uncover the role of bacterial resistance to CST in disease states such as inflammatory bowel disease.

Keywords

Antimicrobial peptide; microbiota; resistance; phosphoethanolamine transferase; omptin

57 **Introduction**

58 The complex microbial community inhabiting the mammalian gut, and in particular their
59 metabolic products, has a crucial effect on various health and disease states, such as
60 inflammatory bowel disorders [1]. Gut microbiota, and its products, are in continuous interaction
61 with the innermost layer of the gut, namely the gut epithelium. Part of the gut epithelial function
62 is to keep the microbes at bay to avoid overstimulation of the underlying immune cells in the
63 gut, and the subsequent inflammation [2,3]. To do so, the gut epithelial cells secrete a wide variety
64 of antimicrobial peptides.

65 CST, a proteolytically processed product of Chromogranin-A (CgA), acts as an antimicrobial
66 peptide [4,5]. The pro-protein CgA is abundantly expressed in endocrine and neuroendocrine cells
67 including the epithelial enteroendocrine cells (EECs) [6–9]. CST consists of 21 amino acid residues
68 and acts on a wide range of regulatory functions including immune, endocrine, metabolic,
69 neurological, and cardiovascular functions [10–14]. For example, mice with a selective deletion of
70 the CST-coding region of the *Chga* gene (CST-KO mice) displayed increased gut permeability,
71 which was restored by CST treatment [15].

72 To date, a few studies have indicated associations between CST and the gut microbiota.
73 Intrarectal administration of CST for 6 days, in mice, resulted in a shift in the gut microbiota
74 composition, with a decrease of *Firmicutes* and an increase in the *Bacteroidota* phyla (Rabbi,
75 Munyaka, and Eissa 2017). These findings suggest the role of CST as a modulator of the gut
76 microbiota composition. This CST-modulatory effect could be mediated by its antimicrobial
77 activity against a wide range of microorganisms. In fact, CST has been reported to have
78 antimicrobial activity against pathogenic bacteria and filamentous fungi in *in-vitro* studies, [5]. In
79 humans, CST showed antimicrobial effects against several skin microbes [16]. Nevertheless, the
80 underlying mechanisms by which CST exerts its effects *in vivo* on the gut microbiota remain
81 obscure. In this study, we show how CST plays a role in governing the colonization of the gut
82 microbiota.

83

Results

Catestatin treatment affects the microbiota composition in CST-KO and WT mice.

The composition of the gut microbiota is shaped by, among others, host-produced antimicrobial peptides [17,18]. Here, we treated CST-KO and WT mice (n=12) with 2 µg/g body weight/day CST by intraperitoneal injection for 15 consecutive days. Amplicon sequencing of the V3-V4 regions of the bacterial 16S gene was performed on the fecal samples of CST-KO and WT mice with and without CST treatment (n=12). Microbial richness, assessed by the observed number of amplicon sequence variants (ASVs) and Chao1 index, showed a significant decrease in CST-KO compared to WT mice **(Figure 1A)**. Interestingly, the richness levels were restored upon treatment of CST-KO mice, but not in WT mice treated with CST. Next, the microbiota diversity was determined by Shannon's *H* and inverted Simpson's index, both indices are used to measure similar parameters of alpha diversity. Similar to the richness scores, the diversity index was significantly higher in the CST-treated CST-KO mice but not in the CST-treated WT group **(Figure 1B).** The data highlight that the effect of the absence of CST in CST-KO mice on the microbiota diversity and richness could be restored upon treatment with CST, while in WT mice, with normal CST levels in their gut, the microbiota diversity and richness did not change with CST treatment.

As a general exploratory analysis, principal component analysis (PCA) was performed and showed distinct clustering of the CST-KO, WT, and CST-treated groups **(Supplementary Figure 1A)**. Particularly, the CST-KO group clustered away from the other 3 groups, while the cluster of CST-treated WT mice showed a great spread and was overlapping with clusters of CST-treated CST-KO mice and WT mice.

To correct for any residual variation in the data, we further employed constrained RDA (redundancy analysis) to determine which bacterial taxa were associated with the different groups of mice at the genus level. The analysis was constrained to both, the mouse genotype and treatment (non-treated and CST-treated). Similar to the cluster separation detected by PCA analysis **(Supplementary Figure 1A)**, both constraints had a significant influence on the model ($p < 0.001$, determined by ANOVA-like permutation test), explaining 13.4% (genotype) and

112 9.8% (treatment) of the variation, respectively (**Figure 1C**). Notably, the CST treated CST-KO
113 group was shifted to the left side along RDA1, indicating a shift in "genotype" upon CST
114 treatment, as opposed to WT, where the treatment group only moved along RDA2, which is
115 associated with the treatment.
116 To assess the treatment effect exclusively on each genotype, we performed RDA constrained to
117 untreated and CST-treated groups. On the genus level, *Dubosiella* and *Romboutsia* showed the
118 strongest association with CST treatment along RDA1 (explaining ~31.2% of the variation) in the
119 CST-KO mice (**Supplementary Figure 1B**). In WT mice, RDA demonstrated an association of
120 *Faecalibaculum, Bifidobacterium, Romboutsia,* and *Anaeroplasma* with the baseline along RDA1
121 (~17.2% explained variance), while *Akkermansia* was more associated with PC1 (~25.1%
122 explained variance; residual variance). *Alloprevotella* and *Candidatus Saccharimonas*
123 representing the strongest associations with CST treatment in WT (**Supplementary Figure 1B**).
124 To further identify which bacterial taxa were affected by the CST treatment, pairwise
125 comparisons of bacterial abundances were performed between CST-treated and untreated groups
126 for each genotype. Focusing on the phylum level, Firmicutes decreased in relative abundance,
127 while Bacteroidota*,* Patescibacteria*,* Desulfobacterota, and Proteobacteria increased with CST
128 treatment in both CST-KO and WT groups. Verrucomicrobiota showed lower abundance in CST-
129 KO but increased significantly in CST-treated groups **(Figure 1D).** The changes depicted on the
130 phyla level in CST-treated WT mice are consistent with findings from Rabbi et al, albeit different
131 CST administration and dosage regimen [19]. These shifts in the main bacterial phyla upon CST
132 treatment was further confirmed to be consistent in human microbiota by *in vitro* culturing of
133 healthy human fecal samples with 10μM CST **(Supplementary Figure 1C).** On family level the
134 most prominent changes were observed for Erysipelotrichaceae, which was consistently
135 decreased in treated groups and Lachnospiraceae, which was increased in CST-KO, but
136 decreased in WT in the CST treated groups. Further Lactobacillaceae was found to be decreased
137 in CST-KO, but increased in WT CST treated groups **(Figure 1D)**.

138 Notably, on the genus level, CST treatment reduced the abundance of *Staphylococcus* and
139 *Turicibacter* in CST-KO and WT mice, while *Alistipes, Akkermansia, and Roseburia,* were
140 significantly increased only in the CST-KO group (**Supplementary Excel Sheet**).
141 Next, we used LEfSe (Linear discriminant analysis Effect Size; Segata et al., 2011) to
142 complement our differential abundance analysis. The main discriminant feature separating the
143 groups (untreated and CST-treated) in CST-KO mice were species from the genera *Atopostipes,*
144 *Jeotgalicoccus, Turicibacter, Staphylococcus,* and Coriobacteriaceae *UCG-002* family **(Figure**
145 **1E)**. In WT mice, the most discriminating genera were *Lactobacillus, Candidatus*
146 *Sacchararimonas, Turicibacter, and Enterococcus***.**
147 Changes in microbial composition are often accompanied by metabolic changes, in particular, the
148 production of short-chain fatty acids (SCFAs) [20]. Thus, levels of SCFAs; acetate, butyrate, and
149 propionate, were measured in the cecum of untreated and CST-treated CST-KO and WT mice
150 **(Figure 1F)**. Remarkably, CST treatment significantly increased the levels of acetate and
151 butyrate in CST-KO mice but not in the WT group. Specifically, butyrate was significantly lower in
152 the CST-KO mice compared to their WT counterparts. Both observations are consistent with the
153 observed significant increase in the SCFA-producing bacteria, *Alistipes, Akkermansia, and*
154 *Roseburia* in the CST-KO group.
155 Overall, the results indicated a significant impact of CST treatment on the diversity and
156 composition of the microbiota in the CST-KO mice, where CST is absent. This effect was much
157 less prominent in WT mice which have normal levels of CST.
158
159 **CST treatment of CST-KO mice promotes the growth of core taxa present in WT mice.**
160 To investigate whether certain taxa exhibit similar behavior (increase or decrease in abundance)
161 between genotypes when CST is administered, we focused on the core microbiota (common taxa
162 between CST-treated groups), representing microbiota members, which directly (e.g., via
163 resistance genes) or indirectly (e.g., via cross-feeding), resist the antimicrobial effect of CST. To
164 do so, log-fold changes between CST treated and untreated groups for both WT and CST-KO
165 mice were compared **(Figure 2)**. Intriguingly, almost all significant changes in core taxa

166 (determined by unpaired Wilcoxon test) were exclusively higher in abundance in CST treated
167 CST-KO mice (quadrants I and II), while, for WT, both significant increases and decreases in the
168 abundance of core taxa were observed. These results coincide with the RDA analysis (cluster of
169 CST-treated CST-KO group moving closer to WT) and indicate that the effect of CST treatment in
170 CST-KO mice promotes the growth of core taxa associated with WT mice. Taxa present in
171 quadrant II, which represent those common taxa between the untreated WT and treated CST-KO
172 mice, are partially restored in their abundance in the latter group. Interestingly, *Turicibacter* was
173 the only core taxon in both genotypes, exclusively negatively affected by CST treatment,
174 exhibiting a significant decrease in abundance and therefore suggesting higher susceptibility to
175 CST. To confirm this observation, we performed *in vitro* assays, to determine minimum inhibitory
176 concentrations (MIC) for *Turicibacter sanguinis*. MIC was also performed for *Bacteroides*
177 *thetaiotaomicron*, which increased in abundance upon CST treatment. The screening revealed
178 low MIC for *T. sanguinis* (32μM CST)*,* while *B. thetaiotaomicron* had a higher MIC (>64 μM CST),
179 thus confirming our *in vivo* observations. Reverse-phase HPLC analysis of spent culture
180 supernatant after 24 hrincubation with CST revealed degradation/uptake of CST from the
181 medium, in the case of *B. thetaiotaomicron,* but not for *T. sanguinis*, hence explaining the higher
182 MIC value in *B. thetaiotaomicron* (**Supplementary Figure 2**). Taken together, the data imply
183 that the changes in the gut microbiota composition associated with the CST treatment **(Figure**
184 **1)** may be caused by the antimicrobial resistance of certain taxa to CST. However, the
185 underlying mechanisms remain obscure.
186

187 **Catestatin treatment promotes the abundance of the gut microbiota harboring**
188 **antimicrobial resistance phosphoethanolamine transferase-encoding genes.**

189 To determine whether bacteria with an increase in abundance in CST-treated groups harbor
190 antimicrobial resistance genes, a metagenomic prediction was performed using PiCRUSt2 on KO
191 (KEGG Orthology) level. From a panel of known AMP resistance genes [21], one KEGG Orthologue
192 (K03760) was found to be significantly different in abundance between CST treated and

193 untreated WT mice and close to significance in CST-KO, when corrected for multiple testing
194 (**Supplementary Excel Sheet**).
195 Sequences within this KEGG Orthogroup contain orthologs of EptA (*E. coli*) phosphoethanolamine
196 transferase. As KEGG Orthologs only contain sequences from reference genomes with no specific
197 gut metagenomic context, we sought to refine our search to investigate the taxonomical
198 distribution of the EptA. To do so, the EptA protein sequence from *E. coli* BW25113 was used as
199 a query to search the Unified Human Gastrointestinal Genome catalog (UHGP). Identified protein
200 sequences were further filtered and clustered into orthogroups using OrthoFinder, to confirm
201 their relationship and exclude any false positives. The analysis revealed 9 orthogroups, while
202 only 5 had more than 2 sequences. The largest orthogroup contained 96% of all protein
203 sequences and was thus used for further analysis. The phylogenetic tree obtained by OrthoFinder
204 exhibited a distinct grouping of sequences without great dispersion, where there was a major
205 subdivision between sequences from the different clades of Bacteroidota, Proteobacteria,
206 Verrucomicrobiota, and Campylobacterota, while sequences of the same phylum were clustered
207 in separate clades **(Figure 3A)**.
208 Using the taxonomical distribution of *eptA,* we reanalyzed the abundance of genera harboring
209 *eptA* upon CST treatment. Remarkably, both CST-treated groups showed a significant increase in
210 microbiota-harboring *eptA*, though the effect in the CST-KO group seemed to be more
211 pronounced **(Figure 3B)**. To further support our findings that *eptA*-harboring core taxa increase
212 in abundance in CST treated groups, we looked at individual log-fold changes of single taxa, as
213 described above **(Figure 2)**. Indeed, *eptA*-harboring core taxa were higher in abundance in CST
214 treated groups, regardless of the genotype **(Supplement Figure 3A)**.
215 Levels of antimicrobial peptides are higher in proximity to the mucosa compared to the lumen [18]
216 . Thus, to replicate our findings in a more physiological environment, we reanalyzed raw
217 sequencing data obtained from a mouse cohort offering paired comparisons between luminal and
218 mucosal microbiota [22]. Intriguingly, a significant increase in the abundance of microbiota
219 harbouring *eptA*-like genes was detected in mucosal samples compared to luminal microbiota

220 **(Figure 3C)**. Notably, this effect was only seen in samples originating from the distal colon, but
221 not from the ileum.
222 To further confirm the bioinformatics analysis outcome for the involvement of the *eptA* gene in
223 CST resistance, wild-type *E. coli* BW25113 and an *eptA* knockout strain (*ΔeptA*) were employed
224 and were cultured in different concentrations (8-100μM) of CST **(Figure 3D).** The results
225 indicate that the lack of *eptA* led to a decreased carrying capacity **(Figure 3D)**, which is
226 equivalent to the maximum population size of the culture, as well as a concentration-dependent
227 prolonged lag-phase during the growth of the *E. coli* **(Figure 3D).**
228 Similar to the majority of known antimicrobial peptides, CST is recognized by the PhoPQ system,
229 which involves the induction of expression of the gene *pmrD*, followed by activation of *pmrA,* and
230 eventually *eptA* expression [23]. To this end, we tested the expression of the above-mentioned
231 transcription regulators in *E. coli* BW25113 strain. Most notably, *phoP* showed approximately 3-
232 fold increase at 0.5 h after stimulation of *E. coli* BW25113 strain stimulated with 20μM CST
233 (sufficient concentration for detection without growth penalty), but only 2-fold and less
234 prolonged in the control, before returning to baseline expression. The *pmrA* showed a later
235 upregulation (after 1h) compared to *phoP* in *E. coli* BW25113 CST-stimulated cultures, while
236 *pmrD* expression spiked in the presence of CST, but was invariant between the different
237 conditions (**Supplementary Figure 3B**).
238 Taken together, the results show a higher abundance of the bacteria-harbouring *eptA*-like genes
239 upon CST treatment, potentially providing these CST-resistant bacteria an advantage to colonize
240 the gut, and, in turn, indirectly affect the colonization of other bacterial taxa.
241

242 **Catestatin peptide is degraded by *E. coli* omptin protease**

243 The ability of *E. coli* BW25113$^{\Delta eptA}$ to still resist comparatively high CST concentrations lead us to
244 test whether the bacterium harbours an additional resistance mechanism, such as degradation or
245 uptake, similar to what we observed in *B. thetaiotaomicron* **(Figure 3D)**. We analyzed the spent
246 culture supernatant by reverse-phase HPLC, which showed absence of CST-corresponding peaks
247 after 24 h of incubation with *E. coli* BW25113$^{\Delta eptA}$ as well as *E. coli* BW25113 **(Supplementary**

248 **Figure 4A)**. To test whether the enzyme involved in the CST degradation is excreted in the
249 supernatant, sterile-filtered supernatants of non-stimulated *E. coli* BW25113 cultures were
250 incubated with CST and subjected to tricine SDS-PAGE to visualize the degradation/uptake of
251 CST. Indeed CST was cleaved by *E. coli* BW25113 after incubation for different time intervals
252 from 30 min up till 24 h **(Figure 4A)**. This suggested the involvement of a secreted or
253 membrane-anchored protease, which can also be present in secreted vesicles, in CST
254 degradation. To identify which protease was involved, literature search was performed and
255 revealed that *E. coli* harbours only 2 major outer membrane proteases, predicted to cleave CST
256 [24]. Among those proteases is the omptin, an outer membrane protease, encoded by *ompT*. To
257 confirm that omptin was responsible for the CST degradation, an *E. coli ompT* knockout strain (*E.*
258 *coli* BW25113$^{\Delta ompT}$) was employed and was cultured in different concentrations of CST. Compared
259 to the wild-type and *E. coli* BW25113$^{\Delta eptA}$ strains, *E. coli* BW25113$^{\Delta ompT}$ showed no growth at
260 100μM CST and an extensively prolonged lag-phase at 64μM (**Figure 3D and Figure 4B)**.
261 Collectively, the results imply that wild-type *E. coli* BW25113 possesses the ability to cleave CST
262 through its outer membrane protease omptin, providing the bacterium with another defense
263 mechanism, together with EptA, to resist the antimicrobial action of CST.
264 To further confirm the complementary function of EptA and omptin, we performed qPCR on
265 control (unstimulated) and CST-stimulated cultures of wild-type *E. coli* BW25113 and *E. coli*
266 BW25113$^{\Delta ompT}$. Intriguingly, *eptA* expression was upregulated about 1.7-fold in *E. coli*
267 BW25113$^{\Delta ompT}$ without CST stimulation compared to the wild-type strain (**Figure 4C**). When
268 stimulated with 20μM CST, an increase in the expression of *ompT,* but not *eptA*, was detected *in*
269 wild-type *E. coli* BW25113 without stimulation and at 0.5 h after stimulation, while this effect
270 was reversed at later time points (**Supplementary Figure 3B**).
271 As *E. coli* BW25113 is considered a lab-strain, which might not be representative of naturally
272 occurring *E. coli* strains, we also tested for the presence of *ompT* in two gut isolate strains,
273 namely *E. coli* Nissle 1917 and *E. coli* DSM 11250. Both were found to be *ompT* carrying
274 (**Supplementary Figure 4B**). Taken together, the results indicate the capacity of *E. coli* strains
275 harbouring omptin to degrade CST, plausibly altering endogenous levels of the peptide in the gut

276 in cases where the abundance of *E. coli* is significantly increased, such as in inflammatory bowel
277 disease [25] To test this hypothesis, we investigated the abundance of *ompT*-like genes (KO term
278 K01355) in different subtypes of inflammatory bowel diseases (IBD), which are also associated
279 with altered levels of CST [15], using publicly available data from the MetaQuery database [26].
280 Remarkably, a significant increase in the abundance of *ompT*-like genes was found between non-
281 IBD and Crohn's disease patients. Similarly, there was a significant increase in the abundance of
282 *ompT*-like genes between Crohn's disease patients and patients with ulcerative colitis, but not
283 between ulcerative colitis diseased and non-IBD subjects (**Figure 4D**). This observation was
284 consistent with the abundance of *E. coli* in those patients (**Figure 4D**). Overall, the data indicate
285 that CST degradation by bacteria-harbouring omptin-like proteases may play a role in altered
286 levels of the peptide previously detected in IBD patients, which, in turn, would result in an
287 overgrowth of these bacteria and worsening of the disease situation.
288

289 **Discussion**

290 This study unravels the crucial role of CST on the microbiota composition in the fecal samples of
291 WT and CST-KO mice. Specifically, there was a significant increase in the abundance of taxa that
292 harbor the CST peptide-resistance enzyme, phosphoethanolamine transferase in CST-KO and WT
293 mice treated with CST **(Figure 3B).** The shifts observed in the microbial phyla in this study after
294 treating WT mice with CST are in agreement with the findings of Rabbi *et al.,* who also reported
295 an increase in *Bacteroidota* and a decrease in *Firmicutes*, albeit a different route for the
296 administration of CST and dosage, (Rabbi, Munyaka, and Eissa 2017). Low abundance of
297 Bacteroidota, especially *Bacteroides*/*Prevotella* have been linked to obesity, and CST-KO mice
298 were described to be insulin resistant and obese besides having elevated blood pressure [13,27]. In
299 contrast, increased *Bacteroidetes/Firmicutes* ratio has been associated with IBD [28,29], which is
300 characterized by elevated levels of CST (Muntjewerff et al., 2021). Nevertheless, as CST is a
301 multifunctional peptide, acting directly on the microbiota as well as on the host, any changes
302 related to CST treatment should be viewed as a complex interplay and not direct causation
303 originating from the microbiota [12].

304 CST treatment could, only to a small extent, restore the microbial composition in a CST-depleted
305 environment, to the composition detected in an environment already primed with CST (WT mice)
306 **(Figure 2)**. In general, the effect of CST treatment observed in the CST-KO group was
307 significantly greater than that in the WT group **(Figure 1)**. This difference could be attributed to
308 the presence of normal levels of CST in the WT mice; thus, the microbiota is already primed with
309 the peptide and has evolved mechanisms to resist its antimicrobial effect. In contrast, the CST-
310 KO group, in which CST is absent, may harbor bacteria that are susceptible to the CST
311 antimicrobial activity but were eradicated upon CST treatment **(Figure 2)**. Especially the core
312 taxa resisting CST treatment seem to benefit from their presence in the gut lumen environment,
313 by exhibiting an increase in abundance. Introduction of CST to a CST-depleted environment did
314 not necessarily promote exclusively health beneficial microbiota, but rather led to a more
315 equilibrated composition, including also pathobiont taxa. For example, in CST-treated CST-KO,
316 *Oscillibacter* and *Mucispirillum* **(Figure 2)**, both of which increased in relative abundance, have

317 been found to increase in diet-induced obesity and might be considered as pathobionts [30,31].
318 Similarly, *Alistipes* was shown to have a detrimental influence on colorectal cancer progression,
319 despite contrasting evidence that it also has protective effects against colitis or cardiovascular
320 diseases [32]. On the other side *Odoribacter*, a SCFA-producer, which increased in relative
321 abundance in CST-treated WT mice **(Figure 2)** has been linked to immunomodulatory effects
322 and general health benefits presumably also in cooperation with *Akkermansia* [33]
323 So far, antimicrobial resistance mechanisms have been mostly investigated in pathogens due to
324 their implication on antibiotic resistance. In *in-vitro* studies, CST has been reported to have an
325 inhibitory effect against the pathogenic gram-positive (*Micrococcus luteus*, *Bacillus megaterium*),
326 gram-negative bacteria (*Escherichia coli* D22), and filamentous fungi (*Neurospora crassa and*
327 *Aspergillus fumigatus)* [5]. Moreover, human CST showed antimicrobial effects against several skin
328 microbes including the gram-positive (*Staphylococcus aureus* and Group A *Streptococcus*),
329 gram-negative bacteria (*E. coli* O29*,* and *Pseudomonas aeruginosa*), also (*Candida albicans)*, and
330 filamentous fungi (*Aspergillus niger, Aspergillus fumigatus, Trichophyton rubrum*) [16].
331 As a defense mechanism, bacteria have evolved several systems to survive the effect of the
332 antimicrobial peptides [21]. The ability to withstand these peptides provides a potential benefit in
333 colonization over other members of the gut microbiota especially under pathological conditions
334 [34]. Analogously, antimicrobial peptides are regularly used by the host to select for specific gut
335 microbiota in homeostatic situations. For CST, the antimicrobial activity resides in the N-terminal
336 of the peptide, which is highly cationic [5]. These positive charges in the peptide interact with the
337 anionic components of the bacterial cell membrane, resulting in the permeabilization of microbial
338 membranes, leading to cell lysis [7]. The present study suggests that CST may as well play a role
339 in aiding the host to select for which microbes to colonize the gut. The abundance of bacteria
340 encoding the phosphoethanolamine transferase genes increased upon CST treatment **(Figure**
341 **3A-E)**. This is not surprising since the *E.coli* phosphoethanolamine transferase e*ptA*, for
342 example, has been linked to colistin resistance, being a cyclic proteinogenic antibiotic [35]. EptA
343 acts by modifying core lipopolysaccharide components with ethanolamine, increasing membrane
344 charge and thus, repelling the antimicrobial agent. The fact that EptA-like proteins are abundant

345 across a variety of different taxa present in the human gastrointestinal tract **(Figure 3A-C)**
346 implies that antimicrobial resistance is a mutualistic and important component in the selection of
347 a specific microbiota composition by the host, through active modulation of antimicrobial peptide
348 levels, such as CST. Indeed, this paradigm is supported by our findings that CST treatment
349 induced a large-scale alteration in the microbiota composition not only in the CST-KO group but
350 also in the WT group, both of which clustered closer to each other, and further away from the
351 untreated groups **(Figure 1)**.
352 The induced expression of *eptA* gene in *E. coli* BW25113$^{\Delta ompT}$ **(Figure 4C)** implies a
353 complementary mechanism when other defense mechanisms are missing. Indeed, we uncovered
354 the degradation of CST by wild-type *E. coli*, a member of the gut microbiota via omptin, an outer
355 membrane protease, known to cleave other cationic antimicrobial peptides, such as protamine or
356 LL-37 [36,37]. The presence of these fragments with high proteolytic activity in the gut has its
357 implications on the microbiota composition, as it may facilitate colonization of other CST-
358 susceptible bacteria [38], in particular, among the mucus-attached bacteria **(Figure 3C)**, where
359 CST levels are higher compared to the luminal CST levels [18]. It remains elusive though, whether
360 CST is taken up and accumulating inside the bacteria or is further degraded, and what the fate of
361 the resulting cleavage fragments is, e.g., through uptake by other microbiota or interaction with
362 the host. Analogously it remains unclear how other bacteria, such as *B.thetathiomicron* can
363 degrade CST **(Supplementary figure 2)** and how widespread such a phenomenon is among the
364 gut bacteria.
365 Levels of CST are increased in IBD patients, while *E. coli* was associated with the development
366 and progression of different IBD types [25,39]. The higher abundance of *ompT*-like genes in samples
367 from Crohn's disease patients, which coincided with a higher abundance of *E.coli* **(Figure 4D)**,
368 suggests that bacteria harboring *ompT*-like genes, such as *E. coli,* may have a benefit to colonize
369 the gut due to its ability to resist CST. In cases where the overall microbial composition is
370 compromised, and the endogenous levels of CST are altered, like in IBD, such bacterial
371 resistance may cause particular bacterial strains to be involved in worsening the gut
372 inflammation. Overgrowth of gut bacteria with the capacity to resist CST may lead the host to

373 secrete higher levels of CST as a defense mechanism. The levels of CST were reported to be
374 higher in IBD patients compared to healthy subjects [15]. It remains unclear why only samples
375 from Crohn's disease patients but not ulcerative colitis showed a higher abundance of *ompT* as
376 well as *E. coli.* One plausible explanation could be due to the different *E. coli* strains
377 predominantly present in either Crohn's disease or ulcerative colitis [40]**(Figure 4D)**.
378 Overall, the present study highlights the significant role of the CST peptide in determining the
379 microbiota composition. The fact that gut bacteria with a capacity to resist the antimicrobial
380 effect of CST become more abundant upon CST treatment, suggests that these bacteria may
381 have gained an advantage over other microbiota members to survive the gut environment,
382 which, indirectly shapes the colonization of the total community. One limitation of the present
383 study is the relatively uncontrolled actual concentrations of CST that eventually reach the gut
384 after intraperitoneal injection. This concentration variability could increase interindividual
385 variability in the microbial composition.
386
387
388

389 **Materials and Methods**

390 **Animals**

391 All studies with mice were approved by the University of California San Diego (UCSD) and
392 Veteran Affairs San Diego Healthcare System (VASDHS) Institutional Animal Care and Use
393 Committees for the Mahata laboratory (UCSD: #S00048M; VA: #A13-002) and were performed
394 in San Diego in adherence to the NIH Guide for the Care and Use of Laboratory Animals. Twelve
395 male adult C57BL/6 J mice (age 20-28 weeks) were purchased from Jackson Laboratory (Bar
396 Harbor, ME) and were acclimatized for 5 weeks before experimentation. Additionally, twelve
397 CST-KO mice generated in the Mahata laboratory were used for this experiment. CST-KO mice
398 have a deletion in the 63 bp CST domain from Exon VII of the *Chga* gene [27] in C57BL/6
399 background. Mice from WT and CST-KO groups were injected intraperitoneally once daily with
400 CST (2 μg/g body weight; Genscript Biotech Corporation, Piscataway, NJ) for 15 days based on
401 previous experimentation [15]. Mice were housed in 4 to 5 animals per cage and had free access to
402 water and food (Normal Chow Diet, LabDiet 5001) in temperature and humidity-controlled rooms
403 with a 12-hr light/dark cycle.

404

405 **Determination of short-chain fatty acids (SCFAs) in cecal samples**

406 Cecal samples (100 mg) were suspended in 1 mL of saturated NaCl (36%) solution. An internal
407 standard (50 μL of 10.7 μM 2-methyl butyric acid in MQ water) was added and the samples were
408 homogenized using glass beads. After the addition of 150 μL H_2SO_4 96%, SCFAs were extracted
409 with 3 ml of ether. The ether layer was collected and dried with Na_2SO_4 (150 mg). The
410 supernatant (0.5 μL) was analyzed using gas chromatography with flame ionization detection
411 (Agilent, Santa Clara, California, USA). The system was equipped with a DB FFAP analytical
412 column (30m x 0.53 mm ID, 1.0 μm; Agilent) and helium GC grade (5.6) was used as carrier gas
413 with a constant flow of 4.2 ml/min. The initial oven temperature was held at 100 °C for 3 min,
414 ramped with 4 °C/min to 140 °C (isothermal for 5 min) and further with 40 °C/min to 235 °C

415 (isothermal for 15 min). The resulting chromatograms were processed using ChemStation
416 (Agilent Technologies).
417
418 **DNA isolation and 16S sequencing**
419 DNA isolation was performed on fecal samples that were collected from untreated and CST-
420 treated WT and CST-KO mice. A phenol-chloroform-isoamyl alcohol procedure was used for DNA
421 extraction [41]. Briefly, the pellet was resuspended in 1 ml of lysis buffer (940µl TE buffer, 50 µl
422 SDS 10% and 10 µl Proteinase K 20 mg/ml) in a 2 ml screw cap micro-tube containing a mix of
423 zirconium and glass beads. Then, samples were incubated at 58°C for 1 hour and 150 µl of
424 buffered phenol (Invitrogen, 15513-047) was added. To support lysis, samples were
425 homogenized 3 × 30 sec with 1-min intervals on ice in a mini bead-beater (Biospec, Bartlesville,
426 USA). This was followed by the addition of 150 µl chloroform/isoamyl alcohol (24:1) and
427 centrifuged at 16,000x *g* for 10 min at 4°C. The upper layer, which contains the DNA, was
428 carefully transferred to a clean tube and 300 µl of phenol-chloroform-isoamyl alcohol [25:24:1]
429 was added. Again, the upper layer was transferred to a fresh tube and 300 µl of chloroform-
430 isoamyl alcohol [24:1] was added. To precipitate the DNA, the upper layer was transferred to a
431 new tube and 1 volume of absolute isopropanol and 1/10 volume of 3M sodium acetate was
432 added. Samples were incubated overnight at -20°C. To get the DNA pellet, the samples were
433 centrifuged at 16,000x *g* for 20 min at 4°C. The supernatant was removed and 700 µl of 70%
434 ethanol was added to remove the remaining salts from the pellet. Ethanol was removed and the
435 DNA pellet was air-dried for 30 min before resuspension of the pellet in 100 µl TE buffer. In each
436 step, samples were vigorously mixed using a vortex.
437 Sequencing of the V3-V4 region of the bacterial 16S gene was carried out by Novogene Co. Ltd.
438 Briefly, for sequencing library preparation, raw DNA extracts were diluted to 1 ng/µl in sterile
439 water, and amplicons were generated by PCR (primers 341F and 806R) using a Phusion® High-
440 Fidelity PCR Master Mix (New England Biolabs). Amplification product quality was assessed by gel
441 electrophoreses and samples were pooled in equimolar ratios. Libraries were generated with a
442 NEBNext® UltraTM DNA Library Prep Kit for Illumina and sequencing was carried out on an

443 Illumina 250bp paired-end platform. Initial processing of reads involved trimming of adapters
444 and primers using a Novogene in-house pipeline (Novogene Co. Ltd, Cambridge, UK).
445

446 **Microbiota analysis**

447 Paired-end sequencing reads were filtered, denoised, merged, and classified with the *dada2*
448 package in the statistical programming language R while processing forward and reverse reads
449 separately until merge [42,43]. Briefly, reads were truncated to 220bp and low-quality reads were
450 filtered followed by dereplication. Error models were learned, while manually enforcing the
451 monotonicity of the error function. Reads were denoised and merged with minimal overlap of
452 12bp, while non-merging reads were concatenated. Singletons have been removed before
453 performing bimera removal, followed by read classification using SILVA (V138) as a taxonomical
454 reference database.

455 For downstream analysis, the *phyloseq* and *microbiome* packages were used richness was
456 determined by the number of observed amplicon sequence variants (ASVs) and alpha diversity
457 was assessed via Shannon's *H* and inverted Simpson indexes [44,45]. All ASVs were collapsed on
458 genus level and cumulative sum scaling was applied using *metagenomeSeq* [46]. The resulting
459 genus abundance table served as input for different types of ordinations such as principal
460 component analysis (PCA) or redundancy analysis (RDA). The significance of constraints in
461 constrained RDA was determined by permutation-like ANOVA. Differential abundance was
462 assessed by unpaired Wilcoxon Rank Sum test using $p < 0.05$ as a significance threshold
463 followed by FDR correction.

464 To generate the double log-fold change plot, first, the core microbiota were estimated for each
465 group by filtering raw ASV counts to contain only more than 10 reads and be present in more
466 than 10% of the samples. Next, only taxa intersecting between CST treated groups were
467 selected and analyzed further. Differential abundance was assessed by a Wilcoxon Rank Sum
468 test between treated and untreated groups per genotype and FDR corrected. Only taxa with an
469 adjusted $p < 0.05$ were considered further. Their mean log-fold changes between groups were
470 calculated and plotted against each other.

471 Further LefSe analysis was carried out, adjusting the alpha value for factorial Kruskal-Wallis test
472 and the alpha value for pairwise Wilcoxon tests to 0.01. Additionally, the LDA score threshold
473 was set to 3.0 [47]
474 For the functional analysis, the metagenomic prediction from 16S data was done using PiCRUSt2,
475 using raw ASVs and unnormalized ASV abundances [48]. For this, ASVs were first filtered to have a
476 minimal abundance of 10 reads and to be present in at least 1/10 of the samples. PiCRUSt2 was
477 run with standard parameters and stratification enabled. The metagenomic data was further
478 analyzed by using STAMP v2.1.3 [49]. For statistical analysis, White's non-parametric t-test, two-
479 sided, and Benjamini-Hochberg multiple test correction were used to reveal differences between
480 groups.
481
482 **Phylogenetic analysis**
483 The amino acid sequence of the *E. coli eptA* gene (UniProt P30845) was searched with *hmmscan*
484 from the hmmer suite (v3.3.1; hmmer.org) against a non-redundant dataset Unified Human
485 Gastrointestinal Protein (UHGP) catalog [50]. Hits were filtered on full sequence E-value, excluding
486 all sequences with an E-value greater than 0.5x the median absolute deviation from the median.
487 Additionally, only sequences originating from genomes with >90% completeness and <1
488 contamination were taken into account. Sequences were dereplicated, grouped by assigned
489 species, and subjected to Orthofinder to infer orthologous groups [51]. The largest orthogroup was
490 selected and OrthoFinder produced gene tree was visualized with FigTree (v1.4.4), to aid
491 visibility the tree was pruned using Treemmer (v0.3; with parameter -RTL 0.95) [52]
492
493 **Bacteria and growth inhibition assay**
494 *E. coli* BW25113, BW25113$^{\Delta ompT}$ (JW0554) and BW25113$^{\Delta eptA}$ (JW5730) (**Supplementary Table**
495 **1**) were routinely grown aerobically in Difco Antibiotic Medium 3 (BD, Franklin Lakes, USA) at 37
496 °C degrees without agitation. Bacteria were inoculated from −80 °C stocks and grown overnight.
497 Before the experiment, cultures were diluted at 1:100 in fresh medium from overnight cultures.
498 Five different CST concentrations were tested in triplicates in a 96-well plate. For this, 10µl of a

499 10x concentrated stock of CST were added to 90µl of diluted culture to obtain final
500 concentrations of 8, 16, 32, 64, and 100 µM. Bacterial growth was monitored for 24h at 600nm
501 (OD600) with shaking for 5s every 15 min using a BioTek ELx808 microplate reader (BioTek,
502 Winooski, USA). Growth curves were fit using the *growthcurver* R package (v0.3.0).
503

504 **Tricine SDS-PAGE**

505 Overnight cultures of *E. coli* strains BW25113 and BW25113$^{\Delta ompT}$ **(Supplementary Table x)**
506 were centrifuged at 10,000 g for 10 min at 4°C and the supernatant was collected. The
507 supernatant was further sterile filtered (0.2µm filters) and to 90 µl of supernatant 10 µl of a 10x
508 CST stock was added to reach a final concentration of 100 µM. Aliquots of 20 µl were taken at
509 time points 0.5, 4, and 24h.
510 To visualize CST degradation, culture supernatants were run on Tricine SDS-PAGE following a
511 modified protocol [53]. Briefly, gels consisted out of a 4% stacking gel and a 16% resolving gel
512 both with a cross-linker ratio of 19:1, and were prepared to standard procedure. For sample
513 prep, 10 µl of each sample were mixed with 10 ml of reducing sample buffer (100 mM Tris-HCl,
514 1% SDS, 4% 2-mercaptoethanol, 0.02% Coomassie Brilliant Blue, 24% glycerol) and incubated
515 at 70°C for 5 min. Subsequently, 10 µl of the sample was loaded on the gel, first, run for ~30
516 min at 30V, and then at 170V for 90 min. Silver staining was applied to visualize proteins using
517 various modifications in fixation to avoid loss of small proteins [54]. For this, gels were fixed (30%
518 ethanol, 15% formalin, 5% acetic acid) for 60 min and quickly washed once with 50% ethanol
519 and twice with MilliQ-filtered water. Gels were incubated for 40 min in 0.005% sodium
520 thiosulfate, followed by incubation for 40 min in 0.1% silver nitrate solution containing 0.07%
521 formalin. Washing with MilliQ-filtered water was performed and a 2% sodium carbonate solution
522 containing 0.1% formalin was added. Gels were incubated for 1-2 min until bands became visible
523 and development was stopped by removing the developer and adding 50 mM EDTA solution. Gels
524 were then imaged in a BioRad ChemiDoc MP Imaging System (BioRad, Hercules, USA).
525

526 **Expression analysis**

527 Overnight cultures of *E. coli* BW25113, *E. coli* BW25113$^{\Delta eptA}$, and *E. coli* BW25113$^{\Delta ompT}$ were
528 resuspended 1:1000 in 6 ml of fresh Difco Antibiotic Medium 3 and grown until OD600 0.5 was
529 reached. Aliquots of 1 ml were harvested, centrifuged at 10,000 g for 10 min, and immediately
530 stored at -80 °C. This and all subsequent centrifugation steps were done at 4 °C.

531 For culture stimulation with CST *E. coli* BW25113 or *E. coli* BW25113$^{\Delta ompT}$ was resuspended
532 1:1000 in 6 ml fresh Difco Antibiotic Medium 3 and grown until OD600 0.5. An aliquot of 5 ml
533 was harvested and centrifuged at 3,000 g for 10 min. The pellet was resuspended in fresh
534 medium containing 20µM CST and gently mixed. Samples of 1 ml were taken at time points 0h
535 (before resuspension), 0.5h, 1h, 2h, and 4h, subsequently centrifuged at 10,000 g for 10 min
536 and immediately stored at -80 °C.

537 RNA was isolated using a phenol:chloroform:isoamyl alcohol procedure as previously described
538 [55]. Briefly, the harvested bacterial pellet was resuspended in 200 µl TE buffer and transferred to
539 a tube containing 0.5g of 0.1 mm zirconia/silica beads, 25 µl 10% SDS, and 200 µl
540 phenol:chloroform:isoamyl alcohol solution. Samples were treated 3 times for 40 s in a mini
541 bead beater and cooling on ice between intervals. Centrifugation for 10 min at 12,500 g was
542 carried out and the aqueous phase was collected and transferred to a tube containing 250 µl
543 chloroform:isoamyl alcohol. Samples were again centrifuged for 5 min at 12,500 g. RNA was
544 cleaned with an RNeasy Mini Kit (Qiagen, Hilden, Germany). For this, the aqueous phase was
545 transferred to a tube containing 700 µl buffer RLT and mixed. Absolute ethanol (500 µl) was
546 added and the mixture was subjected to spin columns. They were centrifuged and washing was
547 performed by adding 350 µl of solution RW1 and centrifuged. 80 µl of DNAse were added (8 µl
548 DNAse buffer, 2 µl DNAse, 70 µl DEPC treated water; Roche, Mannheim, Germany) and
549 incubated for 20 min. Again 350 µl were added, centrifuged, and two times 500 µl of solution
550 RPE were added with centrifugation in between. Columns were spun dry and RNA was eluted
551 with 30 µl of nuclease-free water. The isolates were stored at -80°C until further use.

552 qPCR was carried out according to standard procedures [56]. Briefly, 2 µg of RNA were reverse
553 transcribed using a High-Capacity cDNA Reverse Transcription Kit with RNAse Inhibitor (Applied

554 Biosystems, Vilnius, Lithuania). Subsequently, 10 ng of cDNA were used for qPCR employing a
555 PowerUp SYBR Green Master Mix (Applied Biosystems, Vilnius, Lithuania) and primers for genes
556 *eptA, ompT, phoP, pmrD, pmrA* and *tus*. Reactions were performed in a clear 96-well plate using
557 a BioRad CFX96 Real-Time PCR System (BioRad, Hercules, USA). Gene expression was assessed
558 by normalizing to housekeeping gene *tus* using the R package *qpcR* (v1.4) for curve fitting and
559 the *pcr* (v1.2.2) package for differential expression calculation employing the $2^{-\Delta\Delta Ct}$ method as
560 described in [57].
561
562 **Statistical analysis**
563 All statistical tests were performed using GraphPad Prism 7 or the statistical programming
564 language R. Specific statistical tests are indicated in the text or figure legends. Normality was
565 assessed by either D'Augustino-Pearson omnibus normality test or Shapio-Wilk normality test. If
566 normality was met a t-test was chosen, otherwise non-parametric Mann-Whitney was used.
567 Outliers were assessed with GraphPads ROUT method (Q=1).
568
569 **Data availability statement**
570 All data generated or analyzed during this study are included in this manuscript and its
571 supplementary information files. The 16s rDNA metagenomic sequence data were deposited
572 under BioProject number PRJNA741992.
573
574 **Authors' Contributions**
575 P.G-D., M.S, S.E.A and S.K.M conceived and designed the study. P.G-D., M.S., B.D, and S.K.M.
576 performed the experiments, and P.G-D., M.S, B.D., and S.E.A analyzed the data. P.G-D, M.S,
577 S.E.A. wrote the original manuscript that was reviewed by A.D, B.D., K.V., and S.K.M. Funding
578 for these studies were acquired by S.E.A. and S.K.M. All authors read and approved the final
579 manuscript.
580
581 **Acknowledgment**

582 P.G-D thanks the National Council of Science and Technology in Mexico (CONACyt) for the Ph.D.
583 grant assigned to CVU 690069. We thank Dr. Matthias Heinemann of Department of Molecular
584 Systems Biology, University of Groningen, the Netherlands, for providing us *ΔeptA* and *ΔompT E.*
585 *coli* BW25113 mutant strain; Dr. Greet Vandermeulen of Department of chronic diseases and
586 metabolism, Faculty of Medicine, KU Leuven, Belgium for the help with SCFAs analysis.
587

588 **Funding**

589 S.E.A is supported by a Rosalind Franklin Fellowship, co-funded by the European Union and the
590 University of Groningen, The Netherlands. S.K.M. is supported by a Merit Review Grant (I01
591 BX003934) from the Department of Veterans Affairs, USA.
592

593 **Conflict of interest**

594 The authors declare no competing interests.
595

596 **References**

597 1. Kåhrström CT, Pariente N, Weiss U. Intestinal microbiota in health and disease.
598 Nature2016;

599 2. El Aidy S, van Baarlen P, Derrien M, Lindenbergh-Kortleve DJ, Hooiveld G, Levenez F,
600 Doré J, Dekker J, Samsom JN, Nieuwenhuis EES, et al. Temporal and spatial interplay
601 of microbiota and intestinal mucosa drive establishment of immune homeostasis in
602 conventionalized mice. Mucosal Immunol 2012; 5:567–79.

603 3. Okumura R, Takeda K. Roles of intestinal epithelial cells in the maintenance of gut
604 homeostasis. Exp. Mol. Med.2017;

605 4. Mahata SK, O'Connor DT, Mahata M, Yoo SH, Taupenot L, Wu H, Gill BM, Parmer RJ.
606 Novel autocrine feedback control of catecholamine release: A discrete chromogranin A
607 fragment is a noncompetitive nicotinic cholinergic antagonist. J Clin Invest 1997;

608 5. Briolat J, Wu SD, Mahata SK, Gonthier B, Bagnard D, Chasserot-Golaz S, Helle KB,
609 Aunis D, Metz-Boutigue MH. New antimicrobial activity for the catecholamine release-
610 inhibitory peptide from chromogranin A. Cell Mol Life Sci 2005; 62:377–85.

611 6. Lugardon K, Raffner R, Goumon Y, Corti A, Delmas A, Bulet P, Aunis D, Metz-Boutigue
612 MH. Antibacterial and antifungal activities of vasostatin-1, the N-terminal fragment of
613 chromogranin A. J Biol Chem 2000; 275:10745–53.

614 7. Aslam R, Atindehou M, Lavaux T, Haïkel Y, Schneider F, Metz-Boutigue M-H.
615 Chromogranin A-Derived Peptides Are Involved in Innate Immunity. Curr Med Chem
616 2012; 19:4115–23.

617 8. Angela MD amic., Ghinassi B, Izzicupo P, Manzoli L, Di Baldassarre A. Biological
618 function and clinical relevance of chromogranin A and derived peptides. Endocr.
619 Connect.2014; 3.

620 9. Winkler H, Fischer-Colbrie R. The chromogranins A and B: The first 25 years and
621 future perspectives. Neuroscience 1992; 49:497–528.

622 10. Mahata SK, Corti A. Chromogranin a and its fragments in cardiovascular,
623 immunometabolic, and cancer regulation. In: Annals of the New York Academy of
624 Sciences. 2019.

625 11. Corti A, Marcucci F, Bachetti T. Circulating chromogranin A and its fragments as
626 diagnostic and prognostic disease markers. Pflugers Arch. Eur. J. Physiol.2018;

627 12. Mahata SK, Mahata M, Fung MM, O'Connor DT. Catestatin: A multifunctional peptide
628 from chromogranin A. Regul Pept 2010; 162:33–43.

629 13. Ying W, Mahata S, Bandyopadhyay GK, Zhou Z, Wollam J, Vu J, Mayoral R, Chi NW,
630 Webster NJG, Corti A, et al. Catestatin inhibits obesity-induced macrophage
631 infiltration and inflammation in the liver and suppresses hepatic glucose production,
632 leading to improved insulin sensitivity. Diabetes 2018;

633 14. Mahata SK, Kiranmayi M, Mahapatra NR. Catestatin: A Master Regulator of
634 Cardiovascular Functions. Curr Med Chem [Internet] 2018; 25:1352–74. Available
635 from: https://www.eurekaselect.com/151858/article

636 15. Muntjewerff EM, Tang K, Lutter L, Christoffersson G, Nicolasen MJT, Gao H, Katkar
637 GD, Das S, ter Beest M, Ying W, et al. Chromogranin A regulates gut permeability via
638 the antagonistic actions of its proteolytic peptides . Acta Physiol 2021;

639 16. Radek KA, Lopez-Garcia B, Hupe M, Niesman IR, Elias PM, Taupenot L, Mahata SK,
640 O'Connor DT, Gallo RL. The neuroendocrine peptide catestatin is a cutaneous
641 antimicrobial and induced in the skin after injury. J Invest Dermatol [Internet] 2008;
642 128:1525–34. Available from: http://dx.doi.org/10.1038/sj.jid.5701225

643 17. Bevins CL, Salzman NH. Paneth cells, antimicrobial peptides and maintenance of

644 intestinal homeostasis. Nat Rev Microbiol 2011; 9:356–68.

645 18. Dupont A, Heinbockel L, Brandenburg K, Hornef MW. Antimicrobial peptides and the
646 enteric mucus layer act in concert to protect the intestinal mucosa. Gut Microbes
647 [Internet] 2014; 5:761–5. Available from:
648 http://www.tandfonline.com/doi/full/10.4161/19490976.2014.972238

649 19. Rabbi MF, Munyaka PM, Eissa N, Metz-Boutigue MH, Khafipour E, Ghia JE. Human
650 catestatin alters gut microbiota composition in mice. Front Microbiol 2017; 7.

651 20. Tsukuda N, Yahagi K, Hara T, Watanabe Y, Matsumoto H, Mori H, Higashi K, Tsuji H,
652 Matsumoto S, Kurokawa K, et al. Key bacterial taxa and metabolic pathways affecting
653 gut short-chain fatty acid profiles in early life. ISME J [Internet] 2021; 15:2574–90.
654 Available from: http://dx.doi.org/10.1038/s41396-021-00937-7

655 21. Nuri R, Shprung T, Shai Y. Defensive remodeling: How bacterial surface properties
656 and biofilm formation promote resistance to antimicrobial peptides. Biochim Biophys
657 Acta - Biomembr [Internet] 2015; 1848:3089–100. Available from:
658 http://dx.doi.org/10.1016/j.bbamem.2015.05.022

659 22. Jakobsson HE, Rodríguez-Piñeiro AM, Schütte A, Ermund A, Boysen P, Bemark M,
660 Sommer F, Bäckhed F, Hansson GC, Johansson ME. The composition of the gut
661 microbiota shapes the colon mucus barrier. EMBO Rep 2015; 16:164–77.

662 23. Samantha A, Vrielink A. Lipid A Phosphoethanolamine Transferase: Regulation,
663 Structure and Immune Response. J Mol Biol [Internet] 2020; 432:5184–96. Available
664 from: https://doi.org/10.1016/j.jmb.2020.04.022

665 24. Gottesman S. Proteases and their targets in Escherichia coli. Annu Rev Genet 1996;
666 30:465–506.

667 25. Mirsepasi-Lauridsen HC, Vallance BA, Krogfelt KA, Petersen AM. Escherichia coli

668 Pathobionts Associated with Inflammatory Bowel Disease. Clin Microbiol Rev 2019;
669 32:1–16.

670 26. Nayfach S, Fischbach MA, Pollard KS. MetaQuery: A web server for rapid annotation
671 and quantitative analysis of specific genes in the human gut microbiome.
672 Bioinformatics 2015; 31:3368–70.

673 27. Ying W, Tang K, Avolio E, Schilling JM, Pasqua T, Liu MA, Cheng H, Gao H, Zhang J,
674 Mahata S, et al. Immunosuppression of Macrophages Underlies the Cardioprotective
675 Effects of CST (Catestatin). Hypertension 2021;

676 28. Stojanov S, Berlec A, Štrukelj B. The influence of probiotics on the
677 firmicutes/bacteroidetes ratio in the treatment of obesity and inflammatory bowel
678 disease. Microorganisms 2020; 8:1–16.

679 29. Indiani CMDSP, Rizzardi KF, Castelo PM, Ferraz LFC, Darrieux M, Parisotto TM.
680 Childhood Obesity and Firmicutes/Bacteroidetes Ratio in the Gut Microbiota: A
681 Systematic Review. Child Obes 2018; 14:501–9.

682 30. Lam YY, Ha CWY, Campbell CR, Mitchell AJ, Dinudom A, Oscarsson J, Cook DI, Hunt
683 NH, Caterson ID, Holmes AJ, et al. Increased gut permeability and microbiota change
684 associate with mesenteric fat inflammation and metabolic dysfunction in diet-induced
685 obese mice. PLoS One 2012; 7:1–10.

686 31. Herp S, Durai Raj AC, Salvado Silva M, Woelfel S, Stecher B. The human symbiont
687 Mucispirillum schaedleri: causality in health and disease. Med Microbiol Immunol
688 [Internet] 2021; 210:173–9. Available from: https://doi.org/10.1007/s00430-021-
689 00702-9

690 32. Parker BJ, Wearsch PA, Veloo ACM, Rodriguez-Palacios A. The Genus Alistipes: Gut
691 Bacteria With Emerging Implications to Inflammation, Cancer, and Mental Health.

692 Front Immunol 2020; 11:1–15.

693 33. Hiippala K, Barreto G, Burrello C, Diaz-Basabe A, Suutarinen M, Kainulainen V,
694 Bowers JR, Lemmer D, Engelthaler DM, Eklund KK, et al. Novel Odoribacter
695 splanchnicus Strain and Its Outer Membrane Vesicles Exert Immunoregulatory Effects
696 in vitro. Front Microbiol 2020; 11:1–14.

697 34. McPhee JB, Small CL, Reid-Yu SA, Brannon JR, Moual H Le, Coombes BK. Host
698 defense peptide resistance contributes to colonization and maximal intestinal
699 pathology by Crohn's disease-associated adherent-invasive Escherichia coli. Infect
700 Immun 2014; 82:3383–93.

701 35. Xu Y, Wei W, Lei S, Lin J, Srinivas S, Feng Y. An evolutionarily conserved mechanism
702 for intrinsic and transferable polymyxin resistance. MBio 2018; 9:1–18.

703 36. Thomassin JL, Brannon JR, Gibbs BF, Gruenheid S, Le Moual H. OmpT outer
704 membrane proteases of enterohemorrhagic and enteropathogenic Escherichia coli
705 contribute differently to the degradation of human LL-37. Infect Immun 2012;
706 80:483–92.

707 37. Desloges I, Taylor JA, Leclerc JM, Brannon JR, Portt A, Spencer JD, Dewar K,
708 Marczynski GT, Manges A, Gruenheid S, et al. Identification and characterization of
709 OmpT-like proteases in uropathogenic Escherichia coli clinical isolates.
710 Microbiologyopen 2019; 8:1–36.

711 38. Kulkarni HM, Nagaraj R, Jagannadham M V. Protective role of E. coli outer membrane
712 vesicles against antibiotics. Microbiol Res [Internet] 2015; 181:1–7. Available from:
713 http://dx.doi.org/10.1016/j.micres.2015.07.008

714 39. Muntjewerff EM, Dunkel G, Nicolasen MJT, Mahata SK, Van Den Bogaart G. Catestatin
715 as a target for treatment of inflammatory diseases. Front. Immunol.2018; 9.

716 40. Mirsepasi-Lauridsen HC, Vallance BA, Krogfelt KA, Petersen AM. Escherichia coli
717 Pathobionts Associated with Inflammatory Bowel Disease. Clin Microbiol Rev
718 [Internet] 2019; 32:1–16. Available from:
719 https://journals.asm.org/doi/10.1128/CMR.00060-18

720 41. Santella RM. Approaches to DNA/RNA extraction and whole genome amplification. In:
721 Cancer Epidemiology Biomarkers and Prevention. 2006.

722 42. Callahan BJ, McMurdie PJ, Rosen MJ, Han AW, Johnson AJA, Holmes SP. DADA2:
723 High-resolution sample inference from Illumina amplicon data. Nat Methods 2016;
724 13:581–3.

725 43. R Core Team. R: A Language and Environment for Statistical Computing [Internet].
726 2019; Available from: https://www.r-project.org/

727 44. Lahti L, Shetty S. microbiome R package [Internet]. Available from:
728 http://microbiome.github.io

729 45. McMurdie PJ, Holmes S. Phyloseq: An R Package for Reproducible Interactive Analysis
730 and Graphics of Microbiome Census Data. PLoS One 2013; 8.

731 46. Paulson JN, Colin Stine O, Bravo HC, Pop M. Differential abundance analysis for
732 microbial marker-gene surveys. Nat Methods 2013; 10:1200–2.

733 47. Segata N, Izard J, Waldron L, Gevers D, Miropolsky L, Garrett WS, Huttenhower C.
734 Metagenomic biomarker discovery and explanation. Genome Biol [Internet] 2011;
735 12:R60. Available from: http://genomebiology.com/2011/11/6/R60

736 48. Douglas GM, Maffei VJ, Zaneveld JR, Yurgel SN, Brown JR, Taylor CM, Huttenhower C,
737 Langille MGI. PICRUSt2 for prediction of metagenome functions. Nat Biotechnol
738 [Internet] 2020; 38:685–8. Available from: http://www.nature.com/articles/s41587-
739 020-0550-z

740 49. Parks DH, Tyson GW, Hugenholtz P, Beiko RG. STAMP: Statistical analysis of
741 taxonomic and functional profiles. Bioinformatics 2014; 30:3123–4.

742 50. Almeida A, Nayfach S, Boland M, Strozzi F, Beracochea M, Shi ZJ, Pollard KS,
743 Sakharova E, Parks DH, Hugenholtz P, et al. A unified catalog of 204,938 reference
744 genomes from the human gut microbiome. Nat Biotechnol [Internet] 2021; 39:105–
745 14. Available from: http://dx.doi.org/10.1038/s41587-020-0603-3

746 51. Emms DM, Kelly S. OrthoFinder: phylogenetic orthology inference for comparative
747 genomics. Genome Biol [Internet] 2019; 20:238. Available from:
748 https://genomebiology.biomedcentral.com/articles/10.1186/s13059-019-1832-y

749 52. Menardo F, Loiseau C, Brites D, Coscolla M, Gygli SM, Rutaihwa LK, Trauner A, Beisel
750 C, Borrell S, Gagneux S. Treemmer: A tool to reduce large phylogenetic datasets with
751 minimal loss of diversity. BMC Bioinformatics 2018; 19:1–8.

752 53. Haider SR, Reid HJ, Sharp BL. Tricine-SDS-PAGE [Internet]. 2012. page 81–
753 91.Available from:
754 http://books.google.com/books?hl=en&lr=&id=nBMjPxgHnH0C&oi=fnd&pg=PR5&dq=
755 Malaria+Methods+and+Protocols&ots=X32bRN1-KD&sig=--
756 8WJKCD0ayAyYQkVRKgTS1gVvM

757 54. Schägger H. Tricine-SDS-PAGE. Nat Protoc 2006; 1:16–22.

758 55. Zoetendal EG, Booijink CCGM, Klaassens ES, Heilig HGHJ, Kleerebezem M, Smidt H,
759 de Vos WM. Isolation of RNA from bacterial samples of the human gastrointestinal
760 tract. Nat Protoc 2006; 1:954–9.

761 56. Zhou K, Zhou L, Lim Q, Zou R, Stephanopoulos G, Too HP. Novel reference genes for
762 quantifying transcriptional responses of Escherichia coli to protein overexpression by
763 quantitative PCR. BMC Mol Biol [Internet] 2011; 12:18. Available from:

764 http://www.biomedcentral.com/1471-2199/12/18

765 57. Livak KJ, Schmittgen TD. Analysis of relative gene expression data using real-time
766 quantitative PCR and the 2-ΔΔCT method. Methods 2001; 25:402–8.

767

Figures

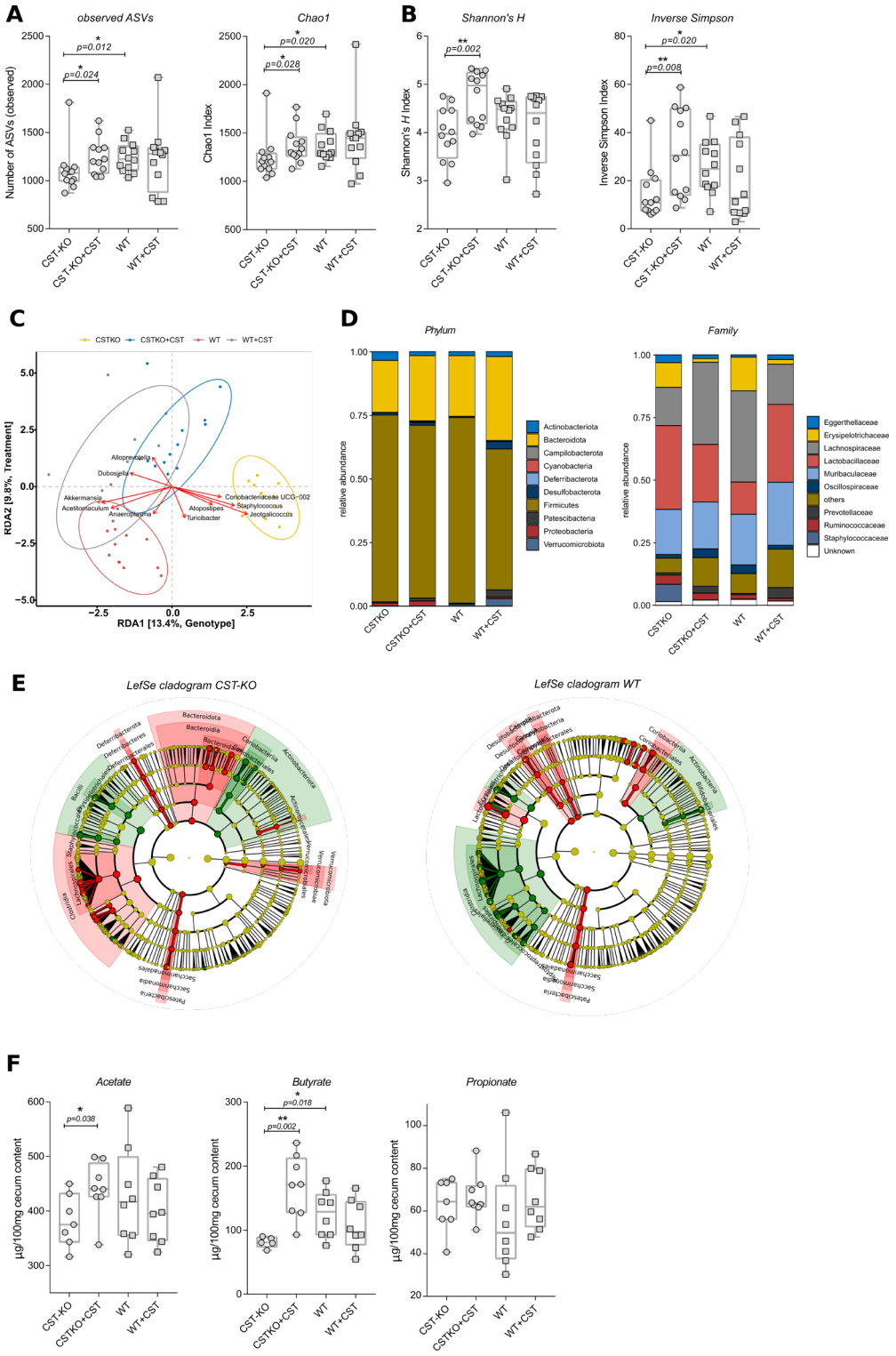
A
observed ASVs
Number of ASVs (observed)
p=0.012
p=0.024
Chao1
Chao1 Index
p=0.020
p=0.028
B
Shannon's H
Shannon's H Index
p=0.002
Inverse Simpson
Inverse Simpson Index
p=0.020
p=0.008
CST-KO
CST-KO+CST
WT
WT+CST
C
CSTKO
CSTKO+CST
WT
WT+CST
RDA2 [9.8%, Treatment]
RDA1 [13.4%, Genotype]
Allopreverella
Dubosiella
Akkermansia
Acetitomaculum
Anaeroplasma
Alopostipes
Turicibacter
Coriobacteriaceae UCG-002
Staphylococcus
Jeotgalicoccus
D
Phylum
Family
relative abundance
Actinobacteriota
Bacteroidota
Campilobacterota
Cyanobacteria
Deferribacterota
Desulfobacterota
Firmicutes
Patescibacteria
Proteobacteria
Verrucomicrobiota
Eggerthellaceae
Erysipelotrichaceae
Lachnospiraceae
Lactobacillaceae
Muribaculaceae
Oscillospiraceae
others
Prevotellaceae
Ruminococcaceae
Staphylococcaceae
Unknown
E
LefSe cladogram CST-KO
LefSe cladogram WT
F
Acetate
Butyrate
Propionate
µg/100mg cecum content
p=0.038
p=0.018
p=0.002

770 **Figure 1. CST treatment affects the murine fecal microbiota.** (**A, B**) Alpha diversity was
771 assessed using different metrics and is concordantly significantly increased upon CST treatment.
772 **(A)** represent the species richness (observed ASVs, Chao1) and (**B**) species diversity of the CST-
773 KO and WT mice before and after CST treatment. Significance was tested with an unpaired
774 *Mann-Whitney* test. Boxes represent the median with interquartile range, and whiskers represent
775 the maxima and minima. (**C**) Genotype and treatment constrained redundancy analysis (RDA) on
776 genus collapsed abundances. Arrows indicate the association of taxa with samples, with the
777 length being a proxy for the strength of the association. Ellipses represent normal data
778 generated by the R package ggplot2. Significant separation of clusters and contribution of the
779 variables to the variance of the RDA was tested with Permutational Multivariate ANOVA
780 (PERMANOVA) and revealed significant ($p < 0.001$) effects of CST administration, both in CST-
781 KO and WT mice; grey – WT+CST, yellow – CST-KO, blue - CST-KO+CST. (**D**) Cladograms of a
782 LefSe analysis (Linear discriminant analysis Effect Size) comparing microbiota changes upon CST
783 treatment in CST-KO and WT mice. Significance was tested using a Kruskal-Wallis (KW) test and
784 Linear Discriminant Analysis (LDA). A significant feature was considered when p-value < 0.01
785 and Log (LDA score) > 3. The green color indicates the microbiota composition before CST
786 treatment and the red color after CST treatment. (**E**) Relative abundance of the present phyla
787 and families (**F**) Concentrations of cecal acetate, butyrate, and propionate, of CST-treated (CST-
788 KO, n=7; WT, n=8) and untreated animals (CST-KO, n=8; WT, n=8). Cecal acetate and butyrate
789 were significantly increased in CST-treated CST-KO mice. Boxes represent the median with
790 interquartile range, and whiskers represent the maxima and minima. Data were analyzed using a
791 2-tailed paired *t*-test. Error bars are shown as mean ± SEM.
792
793

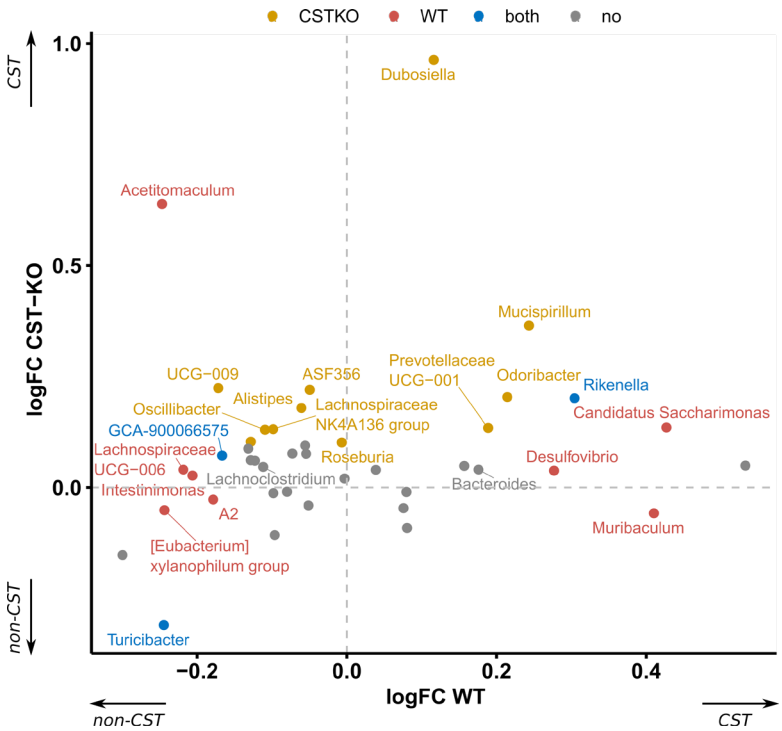

Figure 2 Taxa able to endure CST treatment benefit from its presence in the environment. Scatter plot of log-fold changes, comparing abundance changes for significantly abundant genera between treated and untreated groups per genotype. Colors represent significance when testing for differential abundance between treated and untreated groups for each genotype.

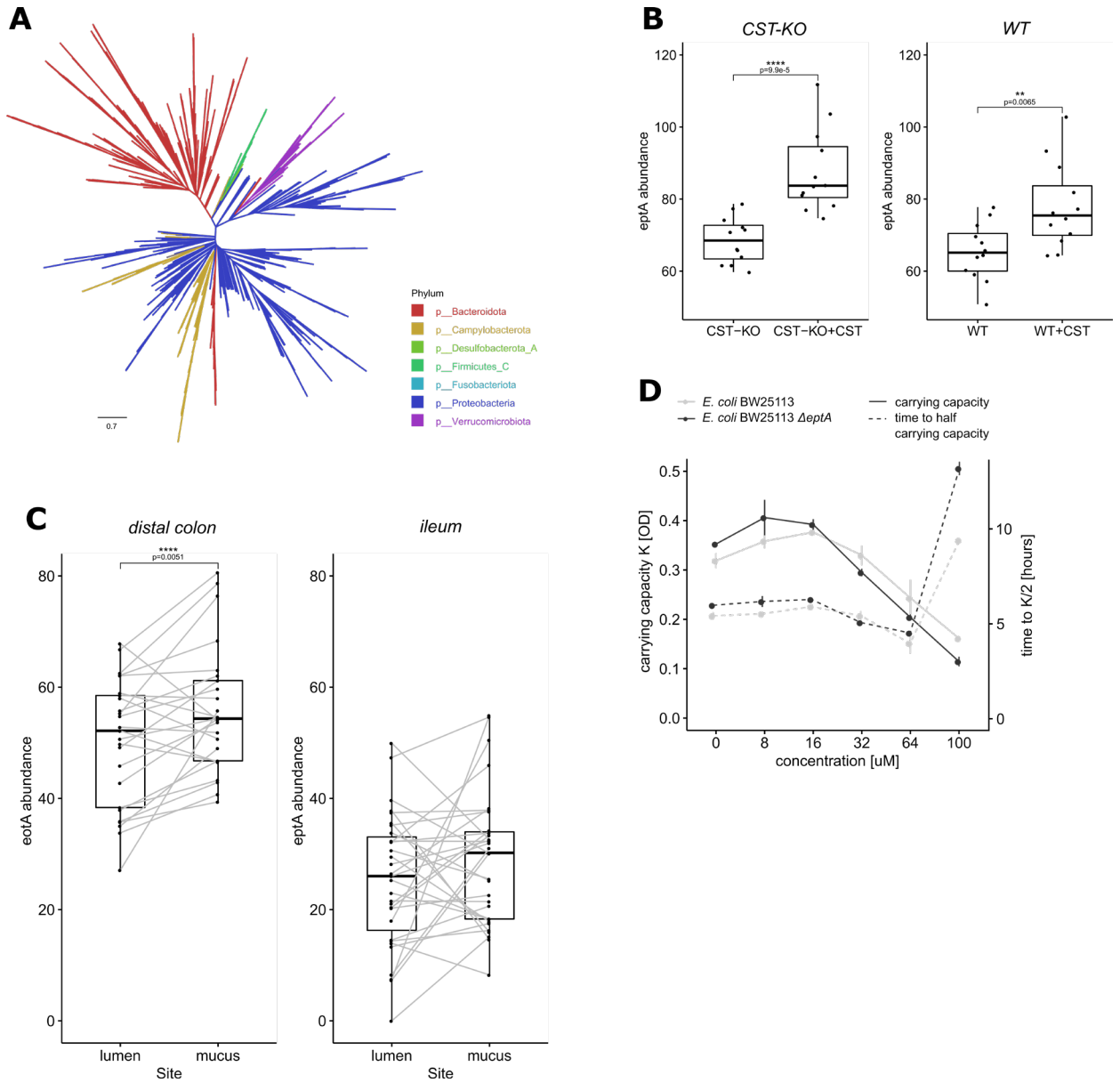

Figure 3. CST treatment promotes the abundance of the antimicrobial resistance gene, *eptA*. (**A**) Unrooted phylogenetic tree depicting the distribution of orthologous *eptA*-like genes throughout bacterial species in the human gut. The tree was pruned to around half its size using Treemmer to aid visualization, while branches were colored by the phylum they belong to. (**B**) Boxplot showing a significant abundance increase of *eptA* harboring bacteria upon CST treatment, both in CST-KO and WT mice. The *eptA* abundance is defined as the sum of abundances from all taxa harboring an *eptA* gene. Boxes represent the median with interquartile range, and whiskers represent the maxima and minima. Significance was assessed by an

811 unpaired *t*-test. (**C**) Significant abundance increase of *eptA*-harboring bacteria in mucus-
812 associated communities, when compared to luminal ones in the distal colon and ileum. Luminal
813 and mucus-associated data is based on **Jakobsson et al. (2015)**. Statistical significance was
814 assessed by paired *t*-test. (**D**) CST inhibits the growth of wild-type *E. coli* BW25113 and *E. coli*
815 BW25113$^{\Delta eptA}$ strains, visualized by carrying capacity K (a measure of maximum OD600) and
816 time taken to reach half the carrying capacity (inflection point of the growth curve at mid-log-
817 phase) that depends on CST concentrations ranging from 8-100 μM.
818
819

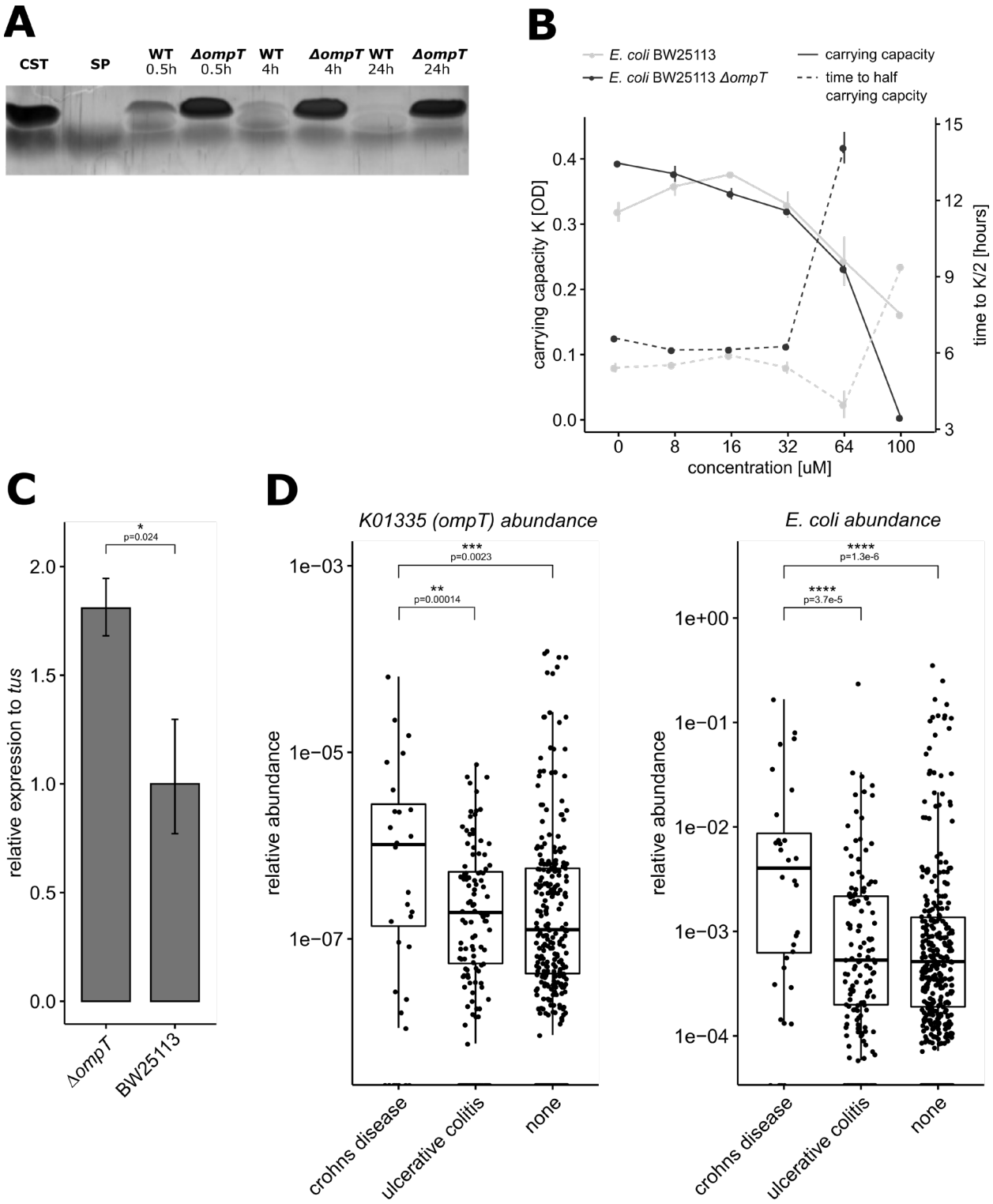

Figure 4. Omptin enzyme is responsible for the degradation of CST in *E coli*. (**A**) Silver-stained tricine SDS-PAGE gels showing the cleavage of CST by wild-type *E. coli* BW25113, but not in *E. coli* BW25113$^{\Delta ompT}$. Sterile non-stimulated culture supernatants were cultured with

824 100μM CST and samples were collected at different time points; CST: catestatin (2.3kDa), SP:
825 substance P (1.3kDa) (**B**) CST inhibits the growth of *E. coli* BW25113$^{\Delta ompT}$, visualized by carrying
826 capacity K (a measure of maximum OD600) and time taken to reach half the carrying capacity in
827 CST concentrations ranging from 8-100 μM. (**C**) Baseline expression of *eptA* is increased in *E.*
828 *coli* BW25113$^{\Delta ompT}$ compared and normalized to that of wild-type *E. coli* BW25113. *tus* was used
829 as a housekeeping gene for normalization in both strains and statistical significance was
830 calculated using a Wilcoxon test. (**D**) Relative abundance of omptin like genes or *E. coli* in
831 patients with Crohn's disease, ulcerative colitis, and healthy subjects. Axes are on log10-scale
832 and significance was assessed using Wilcoxon test without stratification.
833